The Dynamic Catalytic Activity of Phosphorus-containing Catalysts

Han Chen,[1] Jason Gulbinski,[1] Sheetal Jain,[2] Tarnuma Tabassum,[2] Choongsze Lee,[3] Matheus Dorneles de Mello,[4] Nicholas Marcella,[6] Paul Northrup,[7] Anatoly Frenkel,[4,6,8] J. Anibal Boscoboinik,[4,5] Songi Han,[2,5] Susannah L. Scott,[2,5] Michael J. Tsapatsis,[5,9] Wei Fan,[1,5] Omar A. Abdelrahman [1,5*]

[1] Chemical Engineering, University of Massachusetts Amherst, Amherst, MA 01003
[2] Chemistry and Biochemistry, University of California, Santa Barbara, Santa Barbara, CA 93117
[3] Chemical Engineering and Materials Science, University of Minnesota - Twin Cities, Minneapolis, MN 55414
[4] Center for Functional Nanomaterials, Brookhaven National Laboratory, Upton, NY 11973
[5] Catalysis Center for Energy Innovation, University of Delaware, 150 Academy Street, Newark, Delaware 19716
[6] Materials Science and Chemical Engineering, Stony Brook University, Stony Brook, NY 11794
[7] Geosciences, Stony Brook University, Stony Brook, NY 11794
[8] Division of Chemistry, Brookhaven National Laboratory, Upton, NY 11973
[9] Chemical and Biomolecular Engineering, Johns Hopkins University, Baltimore, MD 21218

*Corresponding Author: abdel@umass.edu

Keywords: Phosphorus, Zeolite, Alcohol Dehydration, Hofmann elimination, General Base Catalysis, Amine, Phosphate hydrolysis, Solid Phosphoric Acid

Abstract. The active site speciation of phosphorus-containing all-silica zeolites, P-zeosils, involves a dynamic distribution that is manipulated through controlled hydrolysis of the catalytic material. While water vapor is known to enhance the catalytic activity of phosphorus-based catalysts through phosphorous linkage hydrolysis, here we demonstrate that hydrolysis using a combination of water and sufficiently basic nitrogen-containing compounds like alkylamines increases the acid site density by more than an order of magnitude relative to water-only hydrolysis. The approach of base-assisted hydrolysis was found to be applicable to multiple catalytic chemistries, facilitating both the rates of alcohol dehydration (300× rate enhancement) and alkylamine Hofmann elimination (15× rate enhancement) over P-zeosils. Through a broad array of in situ and ex situ characterization, the enhancement of catalytic activity via base-facilitated hydrolysis was attributed to enhanced acid site density as a result of shifting the dynamic distribution of P-moieties to less condensed states. Specifically, more recalcitrant P-O-P linkages not cleaved through water only hydrolysis, were readily hydrolyzed in the presence of a base. Sufficient basicity in the nitrogen-containing group is critical to access the highest possible density of acid sites, which greatly exceeds that achievable through hydrolysis alone.

1. Introduction. Development of solid catalysts with tunable catalytic activity and selectivity is crucial for heterogeneous catalysis.[1, 2] For solid acid catalysts, acidity can be controlled by incorporation of various heteroatoms in zeolite structures, leading to Brønsted and Lewis acidity

with varying acid strength.[3, 4] Recently, it has been demonstrated that phosphorus-containing catalysts prepared by the impregnation of a siliceous zeolite or silica with phosphoric acid exhibit promising catalytic performance for several biomass upgrading strategies, including *p*-xylene production from cyclo-addition/dehydration of 2,5-dimethylfuran and ethylene, with a yield higher than 95%,[5] as well as renewable lubricants from hydroxyalkylation/alkylation (HAA) of alkylfuran and lauraldehyde with a yield higher than 90%.[6] A more recent reaction of interest is the dehydra-decyclization of biomass-derived furans as a renewable pathway to diene monomers, where butadiene, pentadiene, and isoprene have all been produced with >90% selectivity using phosphorus-containing all-silica zeolites.[7] Near-quantitative yield (95%) of butadiene was also demonstrated over P-containing self-pillared pentasil (P-SPP),[7] although the utility was limited by relatively low catalytic activity. The renewable production of diene monomers and other chemicals over P-zeosils therefore hinges on the ability to develop a more active solid acid, without sacrificing catalytic selectivity. The outstanding selectivity of P-zeosils has been attributed to their mild Brønsted acidity, facilitating the rate-determining ring-opening of furans while avoiding catalyzing subsequent undesirable chemical pathways.[8] As a result, multiple investigations into developing more active dehydra-decyclization catalysts using more conventional and stronger solid acids (aluminosilicates, aluminas, etc.) have been met with limited success.[8] It is therefore imperative to design P-zeosils which retain their milder acidity that affords high selectivity, but also provide higher catalytic activity.

Biomass catalytic upgrading strategies like the dehydration, cycloaddition-dehydration[9, 10] and dehydra-decyclization[8, 11] often involve water as a product. Water is also a major component of biomass feeds, given their inherently high-water content. The presence of water is frequently reported to affect the activity of catalytic materials, including solid acids, where a multitude of mechanistic interpretations have been provided for the observed phenomena.[12-14] Prior studies have indicated that water can specifically increase the catalytic activity of phosphorus-containing catalysts.[15, 16] This is in sharp contrast to more standard solid acids like microporous aluminosilicate zeolites, whose activity is readily inhibited by the presence of water.[17-19] With the desirable catalytic selectivity of P-zeosils for biomass catalytic upgrading, and water's inherent abundance in biomass, understanding the effect of water on the active sites of the phosphorus-containing solid catalysts is indispensable. We therefore sought to leverage water as an in situ modifier, through which the catalytic activity of P-zeosils was modulated. We demonstrate the dynamic nature of phosphorus-containing solid catalysts and their associated catalytic activity, which is readily manipulated in the presence of water and nitrogen-containing molecules like amines, offering significant tunability and enhanced catalytic activity. Water and amines were found to cooperatively enhance the catalytic activity of P-zeosils through active site modulation; the simultaneous presence of both compounds unlocks the full potential of altering the active site speciation of P-zeosils from polyphosphates into less condensed phosphoric acid. The conversion of P species is through hydrolysis of P-O-P and Si-O-P linkages, which increases the acid site density by more than two orders of magnitudes. In contrast, water alone is not capable of hydrolyzing the P-O-P linkages, leading to a much less pronounced activity enhancement. The dynamically evolving phosphorus structures provide an excellent opportunity to control catalytic function and fundamentally understand the catalytic chemistry.

2. Experimental

2.1. Catalyst Synthesis. Phosphorus-containing BEA zeolites (P-BEA) were prepared with dealuminated commercial H-BEA (CP814E, Zeolyst) through previously reported methods.[20] Briefly, Al-BEA was subject to nitric acid treatment to remove aluminum, and 3.35 ml of a H_3PO_4 aqueous solution (0.72 wt % H_3PO_4 for Si/P = 27, and 6.22 wt % H_3PO_4 for Si/P = 3) was added to 0.4 g of dealuminated BEA to achieve the desired Si/P ratio. After drying at 343 K for 1 day, the samples were typically calcined at 873 K with a 1.5 h ramp to 873 K and a 30 min hold at 873 K followed by natural cooling back to room temperature. Air flow (Ultra-zero, Airgas) during calcination was maintained at 100 sccm.

2.2. Catalytic Testing. Kinetic measurements were carried out in a 1/2" quartz downflow packed bed reactor, and the catalyst was placed on a plug of deactivated glass wool (24324, Restek) as support. A ceramic furnace was used to controlled the reactor temperature during pre-treatment (i.e. annealing) using a PID temperature controller (CN 7823, Omega), and both the reactor and the ceramic furnace as well as other parts of the reactor system were placed inside a convection oven (5890 Series II, HP) which controlled the reactor temperature during kinetic measurements. The use of convection oven ensured the absence of temperature gradients across the catalyst bed. A 1/16" type K thermocouple (KQXL-116G-12, Omega) was inserted on top of the catalyst bed to monitor the temperature.

The reactor system consisted of two independent flow paths (flow path 1 and 2) that were connected to the quartz reactor, and each flow path has a vaporization section where the liquid phase reactants were fed into. The vaporization section consisted of a 1/16" stainless-steel capillary line (0.01" I.D., T50C10D, Vici Valco), with one end connected to a 1/16" PEEK capillary line (0.01" I.D., TPK110, Vici Valco) through a PEEK union (ZU1FPK, Vici Valco) and the other end inserted inside the oven. Liquid reactants were fed through the 1/16" PEEK capillary line at controlled rates using a syringe pump (Masterflex EW-74905-04, Cole-Parmer) and air-tight glass syringes (Hamilton Company), and inside the heated vaporization section the liquid was constantly swept by a stream of helium (99.999%, Airgas) and sent to either the reactor or the bypass path. The flow rates of carrier gas on both flow paths were controlled by mass flow controllers (5850S, Brooks Instrument). Helium was purified with a combination of a moisture trap (22014, Restek), an oxygen trap (22010, Restek) and a liquid nitrogen cooled trap before entering the reactor system. The use of a 4-port switching valve (A24UWE, Vici Valco) and a 6-port switching valve (A26UWE, Vici Valco) controlled which flow path was directed to the reactor and the other directed to the bypass vent. Pneumatic actuators were installed on both switching valves for instantaneous switching between flow paths. Both switching valves were placed inside a heated enclosure (HVE2, Vici Valco) to avoid condensation. For kinetic measurement under dry condition, reactant was fed on flow path 1 and dried in situ by passing through a bed of molecular sieve 3Å (regenerated daily at 493 K in 20 sccm of He) before being sent to the catalyst bed. For kinetic measurement under wet condition as well as catalyst activation, reactant/water mixture solutions of certain concentrations were prepared using type 1 water (> 18.2 MΩ cm^{-1}) and were fed on flow path 2. Prior to exposing the catalyst to the reactant stream, all reactants were injected and directed to bypass vent for at least 20 min to obtain a stable reactant partial pressure. Reactor and bypass effluents were analyzed using an on-line gas chromatograph (7890B, Agilent) equipped with a HP-5 capillary column (19091J-413, Agilent) and a flame ionization detector (FID), coupled with a quantitative carbon detector (Polyarc, activated research company). To avoid condensation,

all transfer lines between the reactor outlet and the gas chromatograph were resistively heated to 373 K using Nickel Chromium wire (8880K77, McMaster), insulated with mica wrap sleeving (6811A11, McMaster).

Typically, 0.1 g catalyst was loaded in the quartz downflow packed bed reactor. As pre-treatment, catalysts were annealed in situ in 20 sccm of He at 673 K for 4 h with a ramp rate of 5 K min^{-1}, and then cooled down to reaction temperature before kinetic measurement. All kinetic measurements were performed between 413-513 K at ca. 1.2 bar; pressure drop across the catalyst bed was below 10% of total pressure. The weight hourly space velocity (WHSV) was controlled at 1.8-2.8 $g_{reactant}$ cat^{-1} h^{-1} for all reactants. All carbon balances closed to within ±10%.

2-Propanol (2-PrOH, ≥ 99.5%), tert-butylamine (TBA, ≥ 99.5%), n-butylamine (99.5%), pyridine (99.8%), ammonia/water solution (32%), aniline (99.5%) and 3-fluoropyridine (99%) were purchased from Sigma-Aldrich. Triethylamine (99+%) was purchased from Alfa Aesar. 2-PrOH and TBA were dried with molecular sieves (3 Å beads, 8-12 mesh, Sigma-Aldrich) overnight before use.

2.3. Catalyst Characterization.

2.3.1 X-ray adsorption near edge structure. P-BEA samples were analyzed with X-ray adsorption near edge structure (XANES) spectroscopy at the P K-edge. Spectra were collected at the National Synchrotron Light Source II (NSLS II) at Brookhaven National Laboratory (BNL), using the 8-BM (TES) beamline.[21] Powdered P-BEA samples were finely ground, pressed into pellets, placed into sample stage holder, and covered with polypropylene film (SPEX SamplePrep 3520, 5 μm thick). Samples were loaded into X-ray hutch before filling of hutch with Helium to displace air. Spot size was typically 10 × 10 μm. Phosphorus fluorescence signal was optimized by adjusting sample position to illuminate a representative uniform spot before measurement on each sample. Energy was scanned between 2125 and 2240 eV through 0.1 eV increments using the Si(111) double-crystal monochromator, with the K-edge of the P-BEA samples at approximately 2151 eV. Phosphorus fluorescence was detected via single-element Ge detector ~20 mm from the sample, and normalized to incident beam intensity. Experiments were run at room temperature. Spectra were analyzed with the help of FDMNES theoretical code.[22] FDMNES was used to calculate the P K-edge XANES for H_3PO_4 and P_4O_{10} and an experimental H_3PO_4 standard was used to select the optimal convolution and normalization parameters. The finite difference method (FDM) was used to solve the Schrodinger equation with cluster radii large enough to encapsulate the molecules (2.2 and 4.1 Å were used for H_3PO_4 and P_4O_{10} respectively). The convolution parameters Estart and Efermi were set to -3 and 0 respectively, and the amplitudes of the computed spectra were multiplied by 5.7 to produce the best agreement between the computed and reference H_3PO_4.

2.3.2 Brønsted acid site density. Ex situ measurement of Brønsted acid site (BAS) density was performed through temperature-programmed reaction of the probe molecule, tert-butylamine, to produce isobutene and NH_3. Isobutene was detected and quantified by flame ionization detector (FID) in a modified Gas Chromatography unit, referred to in literature as Reactive Gas Chromatography (RGC).[23] The quartz inlet liner serves as micro-catalytic reactor, HP-PLOT Q column (Agilent19091P-QO4) and FID for signal acquisition and analysis, with a 6-port valve for column bypass. The commercial quartz inlet liner (5190-2293, Agilent) was packed with 20-30 mg of pelletized and sieved catalyst to obtain a particle size of 250-1000 μm to prevent over-

pressurization of the inlet and stacked between 2 quartz wool plugs. Accurate mass of catalyst was obtained by weighing the quartz liner with the bottom quartz wool plug before and after sample addition, as well as the total mass of the fully packed liner, with sample and 2 quartz wool plugs, before and after the experiment. The packed liner was pre-treated at 673 K for 1 h in the inlet under helium, then the inlet temperature set to 423 K until equilibrated for surface saturation. At inlet temperature of 423 K, the TBA was injected using the automated liquid sampler (ALS) with 1 μL of TBA injected at 1-minute intervals, with 15 total injections deemed sufficient to saturate the catalyst surface. Inlet temperature of 423 K was held for 2 h, purging the surface of the catalyst of any physio adsorbed TBA, so that only BAS-associated TBA remained. The 6-port valve was set such that the column was bypassed for catalyst pre-treatment, TBA surface saturation, and purge, so TBA injected in the inlet would flow directly to the FID. Oven temperature was set at 373 K and column flow maintained with helium to not damage the column through oxidation. After the 2 h inlet purge at 423 K, oven temperature was cooled to 303 K, the 6-port valve pneumatically activated to bring the column online with the inlet, and the inlet temperature ramped to 673 K, reactively desorbing the TBA producing isobutene and ammonia, the former of which would be trapped in the column at the over temperature of 303 K. After the inlet reached 673 K, the oven temperature was increased by 10 K min^{-1} to 473 K, eluting the isobutene to be detected by FID. FID was calibrated with standard isobutene gas and ZSM-5 of Si/Al=11.5, 40, and 140, and split ratio verified manually with bubble flow meter.

2.3.3 X-ray photoelectron spectroscopy. X-ray photoelectron spectroscopy (XPS) spectra of powders were collected at room temperature and under UHV (base pressure of 10^{-9} mbar) using a SPECS electron spectrometer system equipped with PHOIBOS NAP 150 hemispherical energy analyzer and a monochromatic Al K_α X-ray source (1486.7 eV). The powdered samples were pressed on copper tape mounted on a stainless-steel flag-type sample holder. Components Si 2p and N 1s and P 2p were collected with 25 scans. C 1 s spectra corresponding to adventitious carbon were used as a reference for further calibration at 284.8 eV. P-BEA-3 sample for XPS measurement was annealed in situ (100 sccm of He) at 673 K for 4 h, cooled down 513 K, and then activated with water and base molecules (tert-butylamine, trimethylamine or ammonia) with P_{base} = 10 Torr, P_{water} = 180 Torr for 2 h. After activation, the sample was either purged in He at 513 K for 1 h, or annealed at a higher temperature (673, 773 or 873 K) to test the effect of annealing temperature on residual N in P-BEA-3.

2.3.4 Infrared spectroscopy. In situ Fourier transform infrared (FT-IR) spectroscopy was performed on a Bruker Tensor II spectrometer equipped with a DLaTGS detector and mid-infrared source. Spectra were collected between 1000 and 6000 cm^{-1} with a 4 cm^{-1} resolution, averaged over 64 scans and subtracted from a background spectrum taken in the absence of sample. 10-15 mg of P-BEA-3 was pressed into 13 mm diameter thin self-supporting catalyst wafers using a pellet press at 20 MPa of pressure for 15 min. The catalyst wafer was then loaded into a custom-built heated transmission cell, equipped with water-cooled CaF_2 windows. The temperature of the cell was controlled using a PID temperature controller (CN 7823, Omega) and a 1/16" type-K thermocouple, with a secondary thermocouple in a thermowell touching the sample wafer to monitor the catalyst temperature. The catalyst was annealed in situ (20 sccm of He) at 673 K for 1 h at a ramp rate of 3 K min^{-1}, and then cooled down to the temperature at which the measurements were performed. Liquid phase reactants/probe molecules were injected using a syringe pump and an air-tight glass syringe to a vaporization section with similar setup described in previous section.

The injected liquid was vaporized by a stream of He whose flow rate was controlled by a mass flow controller (Type 201, Porter). The vapor mixture was directed either to the transmission cell or to the bypass vent line using a 6-port switching valve (A26UWE, Vici Valco) placed within a heated valve enclosure (HVEB, Vici Valco) along with the vaporization section. All transfer lines connected to the transmission cell (sample inlet and outlet) were resistively heated using Nickel Chromium wire with insulating mica wrap sleeving.

2.3.5 Solid-state ^{31}P nuclear magnetic resonance. Room temperature ^{31}P solid-state nuclear magnetic resonance (NMR) experiments were performed at 11.7 T magnetic field, corresponding to a Larmor frequency of 323.85 MHz for ^{31}P spins. Given the hygroscopic nature of P-zeosils, all P-BEA-3 samples were purged in He at 513 K for 2 h post-activation to remove residual water and base molecules, sealed in glass vials under an inert He environment, and transferred into sealed 4.0-mm zirconia NMR rotors in a glovebox. During the NMR measurements, the rotors were spun at 12.5 kHz at the magic angle using dry N_2 as the spinning and bearing gas to avoid exposure to moisture. In all cases, a 7 μs 90 ° pulse was used to excite ^{31}P spins. ^{31}P chemical shifts are referenced to phosphoric acid solution (1 M).

2.3.6 X-ray diffraction. All P-BEA samples were characterized by powder X-ray diffraction analysis (XRD) with a Rigaku SmartLab diffractometer containing Cu-Kα radiation source at 45 kV and 40 mA current with 0.016 step size. Diffractograms were measured from 4 to 40 degrees two-theta.

2.3.7 Surface texture analysis. Nitrogen adsorption−desorption isotherms were measured at 77 K by using an automated gas sorption analyzer (Autosorb iQ2, Quantachrome) after the samples were degassed at 573 K under vacuum for 12 h.

3. Results & Discussion.

3.1. Alcohol dehydration over P-zeosils activated with H_2O and tert-butylamine. We recently demonstrated that alcohol dehydration can be used as a catalytic probe chemistry to kinetically interrogate the surface acidity of P-zeosils.[24] Therefore, 2-propanol (2-PrOH) dehydration was carried out over P-BEA (Si/P = 3, P-BEA-3) to probe water's impact on catalytic activity. An equimolar feed of water and 2-propanol (10 Torr, $P_{2\text{-PrOH}}$:P_{water} = 1) significantly increased the rate of alcohol dehydration relative to dry conditions (~ 7× rate enhancement, **Figure 1A**, green patterned and filled symbols), while the parent aluminosilicate zeolite (Al-BEA) experienced a significant loss in catalytic activity (~30 %) under identical conditions (**Supporting Information, Figure S1**). Product selectivity was not significantly altered in the presence of water; propene was predominantly formed over P-BEA-3 in the presence (selectivity > 97%) and absence (selectivity = 96%) of water, with diisopropyl ether (DIPE) being the only other carbon-containing product. (**Supporting Information, Figure S2**). Selectivity to propene was significantly lower (~60%) over Al-BEA, which we previously demonstrated to be the consequence of a relatively destabilized 2-propanol dimer adsorbate over the catalytic P sites compared to Al sites.[24] Returning P-BEA-3 to dry conditions restored the rate of 2-propanol dehydration observed prior to the introduction of water, suggesting a reversible process. The enhanced catalytic activity of P-BEA in the presence of water is consistent with prior observations over solid phosphoric acid catalysts;

200-1000 ppm of water vapor is necessary to maintain the catalytic activity for typical industrial propene oligomerization, attributed to the hydrolysis of polyphosphoric acid into less condensed forms (ortho- and pyrophosphoric acids).[15] Jichang et al. reported a threefold increase in the acid site density of solid phosphoric acid after treatment with steam.[25] Considering the similar presence of condensed phosphoric acid moieties in P-zeosils,[26] it is likely that water hydrolyzes condensed phosphates in P-BEA-3, leading to a greater density of available phosphorus active sites and a higher overall rate of 2-propanol dehydration. Conversely, the inhibitory effect of water over Al-BEA also indicates that the observed rate enhancement is more related to the nature of the catalyst rather than the probe chemistry itself.

While the impact of water can be rationalized based on phosphate (P-O-P) and silicophosphate (Si-O-P) linkage hydrolysis, it is unclear whether water alone is sufficient to hydrolyze the various phosphorus-based species present on the catalyst surface. For example, base-assisted routes are frequently reported for the hydrolysis of phosphate esters in biological systems.[27-29] Kirby et al. demonstrated that pyridine accelerated the hydrolysis of phosphate diester by more than 3 orders of magnitude, acting as an intramolecular general base that assisted the nucleophilic attack of water.[30] Additionally, Bahia and coworkers reported that siloxide and silanol groups on the surface of bare silica materials, similar to the all-silica support of P-zeosils, induced general base catalysis for water hydrolyzing a phosphate diester.[31] Inspired by these observations, we developed a base-assisted activation of P-zeosils. Prior to catalyzing 2-propanol dehydration, P-BEA-3 was exposed to a vapor phase mixture of tert-butylamine (TBA) and water (P_{TBA} = 10 Torr, P_{water} = 180 Torr, 513 K), then annealed at 673 K in He to desorb any residual tert-butylamine. Here, TBA serves as an organic base that can assist in P-O-X linkage hydrolysis. Relative to the parent catalyst, amine-activated P-BEA-3 exhibited significantly higher rates of 2-propanol dehydration under dry conditions (**Figure 1A**, red patterned symbols, $P_{2\text{-PrOH}}$ = 10 Torr), which further increased by more than a factor of 30 upon co-feeding an equimolar amount of water (**Figure 1A**, red filled symbols, $P_{2\text{-PrOH}}$:P_{water} = 1). Product selectivity on the activated P-BEA-3 remained unaltered relative to the parent catalyst, both in the presence and absence of water. Identical activations of P-BEA-3, but in the absence of either tert-butylamine or water, resulted in no significant change in catalytic activity (**Supporting Information, Figure S3**), demonstrating the necessity for the simultaneous presence of water and amine. Relative to the parent P-BEA-3 catalyst under dry conditions, an exceptionally large rate enhancement of ~ 300× is observed over the amine-activated catalyst in the presence of water (**Figure 1B**). Additionally, elemental analysis via X-ray photoelectron spectroscopy (XPS) revealed no residual nitrogen on amine activated P-BEA-3 after annealing at 673 K in He, confirming that enhanced reaction rates cannot be attributed to residual nitrogen-containing species (**Supporting Information, Table S1**).

3.2. Altering active site density vs nature. Two possibilities were considered for the amine-driven enhancement of catalytic activity: a change in the catalytic activity of alcohol dehydration per phosphorus active site, or an increase in the number of available phosphorus active sites. The former explanation suggests a change in the nature of the active site(s), resulting in a change in the energetics of the catalytic pathway. The rate of alcohol dehydration is known to be strongly affected by acid site strength, and therefore, the nature of the active site.[32, 33] A solvation effect can also be invoked, where water in the pores preferentially stabilizes a kinetically relevant transition state and increases the rate of reaction. However, Lercher et al. examined this possibility for n-propanol dehydration over aluminosilicates and reported that water will destabilize the transition state relative to the reactant state and lead to a reduction in rate.[19] Alternatively, if the activity per

site remains unchanged, the enhanced rate of alcohol dehydration is likely due to an increased active site density from polyphosphate hydrolysis.

To distinguish between these two possible explanations, we performed an in situ kinetic poisoning under dry and wet conditions, using TBA as a poison to measure the acid site density under reaction conditions (**Supporting Information, Figure S4**). We have previously demonstrated that amines poison acid sites on P-zeosils under 2-propanol dehydration reaction conditions, providing an in situ quantification of both the site-time yield of 2-propanol dehydration (i.e., the time-averaged activity per site) and Brønsted acid site density.[24] Briefly, an instantaneous switch is made from a feed of 2-propanol (or 2-propanol and water) to one including a concentration of TBA (0.1 mol %). At the temperature which 2-propanol dehydration was investigated (413 K), TBA is itself unreactive, and acts as an irreversible adsorbate that prohibits 2-propanol from adsorbing and undergoing dehydration. Assuming a stoichiometric adsorption complex (1 mol TBA (mol H^+)$^{-1}$), the decrease in rate normalized by the uptake of TBA provides an in situ estimate of the activity per Brønsted acid site (mol 2-PrOH (mol H^+ s)$^{-1}$). Despite the large difference in the mass-normalized rate of reaction (mol product (g P-BEA s)$^{-1}$) between the parent and TBA activated P-BEA-3 (> 10^2 ×, **Figure 1B**), the in situ estimated rate of 2-propanol dehydration per available active site (mol product (mol H^+ s)$^{-1}$) of the two extremes are near identical (~1.1×, **Figure 1C**). Accordingly, a large increase in Brønsted acid site density was for the TBA-Water-activated catalyst (15700 μmol H^+ (g catalyst)$^{-1}$), relative to the parent P-BEA-3 (48 μmol H^+ (g catalyst)$^{-1}$, **Figure 1C**). Assuming all condensed phosphates are ultimately hydrolyzed into orthophosphoric acid, with three protons per molecule, a theoretical maximum Brønsted acid site density of 16700 μmol H^+ (g catalyst)$^{-1}$ is expected. The large enhancement in the rate of alcohol dehydration, brought about by activating P-BEA-3 with a pre-treatment of co-feeding TBA and water, is therefore consistent with an increase in active site density.

3.3. Nature of activating amine. Under the conditions of activating P-BEA-3 with tert-butylamine and water (513 K), tert-butylamine decomposes to ammonia and isobutene through a Brønsted acid-catalyzed Hofmann Elimination.[34, 35] As a result, ammonia formed through Hofmann elimination may also interact with the catalyst and participate in the activation mechanism. Indeed, an ammonia-water pre-treatment of P-BEA-3 resulted in an identical enhancement in the rate of 2-propanol dehydration in the presence of an equimolar co-feed of water and 2-propanol (**Figure 1D**). However, n-propylamine and triethylamine, which do not undergo Hofmann elimination at the activation temperature, also led to an identical rate enhancement, suggesting that the presence of ammonia is not necessary. Several nitrogen-containing bases were found to be capable of activating P-BEA in the presence of water vapor: tert-butylamine, propylamine, triethylamine, and ammonia all resulted in similar enhancements in the rate of 2-propanol dehydration. Once the basicity of the activating molecule (indicated by bulk aqueous phase values of pK_b at 298 K)[36] decreased to approach that of pyridine (pK_b = 8.8), the measured rate enhancement decreased, until it was no longer observable with weaker bases like aniline (pK_b = 9.4) and 3-fluoropyridine (pK_b = 11.2). The ability to activate the hydrolysis of P-BEA-3 therefore depends on the basicity of the activating molecule.

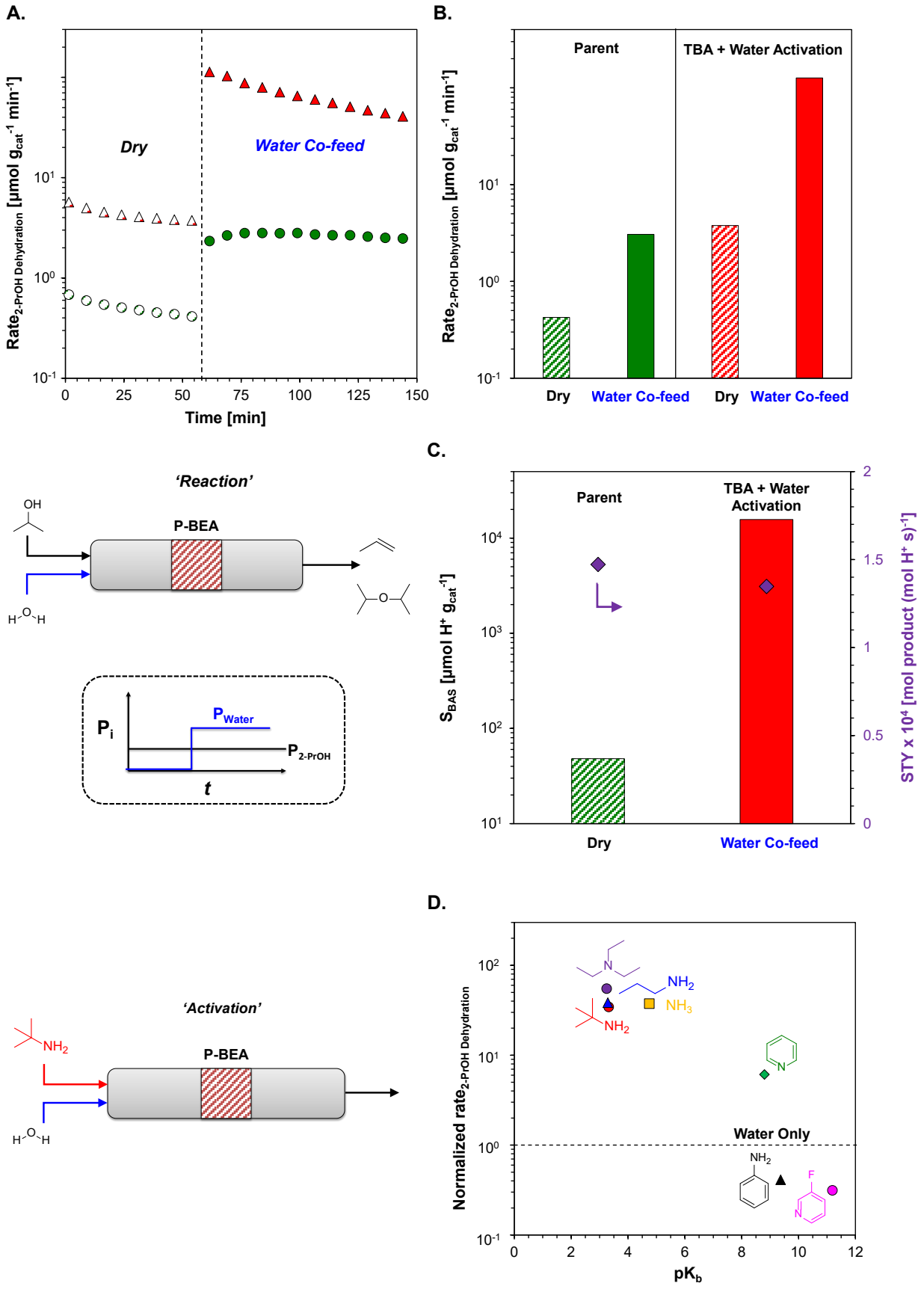

Figure 1. Kinetic measurements of 2-propanol dehydration over P-BEA-3. A. Time-on-stream profiles and **B.** rates of 2-propanol dehydration over parent catalyst (⊘/●) and catalyst activated (△/▲) (by a vapor phase treatment with a mixture of tert-butylamine (TBA) and water followed by He annealing) under dry and water co-feed conditions. Dashed line in **A** indicates the moment an instantaneous switch was made between dry and wet feed streams. Patterned and filled symbols represent rates measured under dry and water co-feed (P_{water} = 10 Torr) conditions, respectively. The schematics depict the 2-PrOH dehydration reaction with and without water co-feed (top) and the amine-and-water activation procedure (bottom) **C.** In situ titration-measured Brønsted acid site densities and 2-PrOH dehydration site-time-yield under dry (patterned) and water co-feed (solid) conditions **D.** Rates of 2-PrOH dehydration under water co-feed condition over P-BEA-3 activated with nitrogen-containing molecules of varying basicity (pK_b), normalized against rate over P-BEA-3 activated with water only. pK_b values are obtained from ref. [36]. All rate measurements of 2-PrOH dehydration were performed at T = 413 K with $P_{2\text{-PrOH}}$ = 10 Torr, and all P-BEA-3 activations were performed at T = 513 K with P_{base} = 10 Torr and P_{water} = 180 Torr.

3.4. In situ tracking of hydrolysis through Hofmann elimination. To better understand the mechanism by which amines facilitate phosphate hydrolysis, we investigated the effect of water on the steady-state Hofmann elimination of alkylamines. We previously demonstrated that the rate of alkylamine Hofmann elimination provides a direct measure of the intrinsic surface rate of reaction, which can be directly correlated to the number of active sites available.[17] TBA forms a stoichiometric adsorption complex over a Brønsted acid site, and its highly exothermic and irreversible adsorption leads to a catalyst surface saturated with TBA.[23, 37] The surface saturation was further confirmed by measurement of reaction kinetics: the rate of Hofmann elimination was completely insensitive to TBA partial pressure over two orders of magnitude (0.5-50 Torr) for both aluminosilicates and P-zeosils (**Supporting Information, Figure S5**), indicating a highly covered surface with no vacant Brønsted acid sites. As a result, the measured rate of Hofmann elimination provides a direct and in situ estimate of Brønsted acid site density available for catalysis. Therefore, in addition to facilitating active site generation through hydrolysis (amine-and-water activation procedure), the specificity and water-free nature of TBA Hofmann elimination provides an ideal reaction environment by which to kinetically interrogate the effect of catalyst activation by hydrolysis.

Over an aluminosilicate, co-feeding water significantly inhibits the rate of Hofmann elimination.[17] Conversely over P-BEA-3, the rate of Hofmann elimination significantly increased in the presence of water, qualitatively consistent with the observed rate enhancement for 2-propanol dehydration. At the activation conditions (513 K and 10 Torr TBA), the rate of tert-butylamine was stable and showed no significant change as a result of activation in the presence of only TBA. Once water was introduced (180 Torr), the rate of TBA Hofmann elimination increased by a factor of 13.4, where it consistently remained (**Figure 2A**). Taking the rate of Hofmann elimination to scale with Brønsted acid site density, the number of available active sites had increased by more than an order of magnitude in the presence of water. Pre-treating P-BEA-3 with an identical partial pressure of water (prior to TBA Hofmann elimination) led to no apparent change in rate (**Supporting Information, Figure S6**), demonstrating the simultaneous need for both amine and water, consistent with observations based on 2-PrOH dehydration (**Section 3.1**). Subsequent removal of water from the feed stream did not lead to any further significant change in catalytic activity; the rate of Hofmann elimination did not return to its original level prior to the introduction of water. This suggests that the change in Brønsted acid site density, presumably as a

result of hydrolysis, is relatively irreversible under reaction conditions of Hofmann elimination. Annealing the catalyst in He at 673 K, however, completely reversed the change induced by water, restoring the rate of Hofmann elimination to that of the parent P-BEA-3 (**Figure 2A**). Re-introducing water to the annealed catalyst resulted in an increase in catalytic activity, identical to that observed during the first hydrolysis cycle.

Exploring the effect of catalyst hydrolysis at lower water partial pressures, a bifurcating behavior emerges. Reducing the partial pressure of water to 10 Torr, does not result in any significant change in the rate of Hofmann elimination over P-BEA-3 (**Supporting Information, Figure S7**). However, subjecting the same P-BEA-3 to a hydrolysis cycle with 180 Torr water first, then annealing at 673 K in He, showed a large increase in rate upon adding 10 Torr water. An initial activation involving a larger partial pressure of water therefore appears to be required for catalyst hydrolysis to be effective. Expanding upon this result, we examined the promotional effect of catalyst hydrolysis over a range of water partial pressures on the activated catalyst (0.1-350 Torr, **Figure 2B**). Even at a relatively low partial pressure of 0.1 Torr water, the rate enhancement observed was a factor of 5.5× relative to the parent P-BEA-3. This demonstrates the substantial impact of hydrolysis on catalytic activity, as a result of converting more condensed P-sites to less condensed P-sites. As the partial pressure of water increased beyond 100 Torr, the incremental rate enhancement begins to decrease and approaches a plateau.

The increase in Brønsted acid site density was further confirmed with in situ Fourier transform infrared spectroscopy (IR) measurements of the N-H vibrational modes of surface tert-butylammonium. Peaks at 1540 and 1629 cm^{-1} are assigned to δ(NH) bending modes of tert-butylammonium (**Supporting Information, Figure S8A and S8B**),[37, 38] while peaks at 1383, 1408 and 1482 cm^{-1} are assigned to δ(CH) bending modes. Assuming all contributions of tert-butylammonium δ(NH) bending modes have the same molar extinction coefficient, integrated areas are directly proportionally to the concentration of protonated tert-butylamine present on the catalyst surface, providing an in situ estimate of Brønsted acid site density. Over P-BEA-3, the integrated area of the peak at 1540 cm^{-1} increased eight-fold in the presence of 180 Torr water, and was sustained once water was removed from the feed (**Figure 2C**). Additionally, an increase in the peak intensity at 3742 cm^{-1}, assigned to the O-H stretching mode of surface-bound silanol groups,[39, 40] was observed after P-BEA-3 was activated and annealed (**Supporting Information, Figure S8C)**. Changes in the peak intensity likely results from P-O-Si linkage hydrolysis during catalyst activation with subsequent formation of P-OH and Si-OH groups:

$$\text{P-O-Si} + H_2O \rightleftharpoons \text{P-OH} + \text{Si-OH} \qquad (1)$$

The in situ IR measurements are consistent with the generation of additional Brønsted acid sites through polyphosphate and silicophosphate linkage hydrolysis into acidic P-OH sites, resulting in the observed rate enhancement in both TBA Hofmann elimination and 2-propanol dehydration. In contrast, no significant change was observed for the integrated δ(NH) bending peak area over H-ZSM-5 when water was co-fed with TBA, suggesting no change in Brønsted acid site density, consistent with the general acknowledgement that the structural framework of aluminosilicate zeolites is more hydrothermally stable and non-dynamic under our reaction conditions.[41, 42]

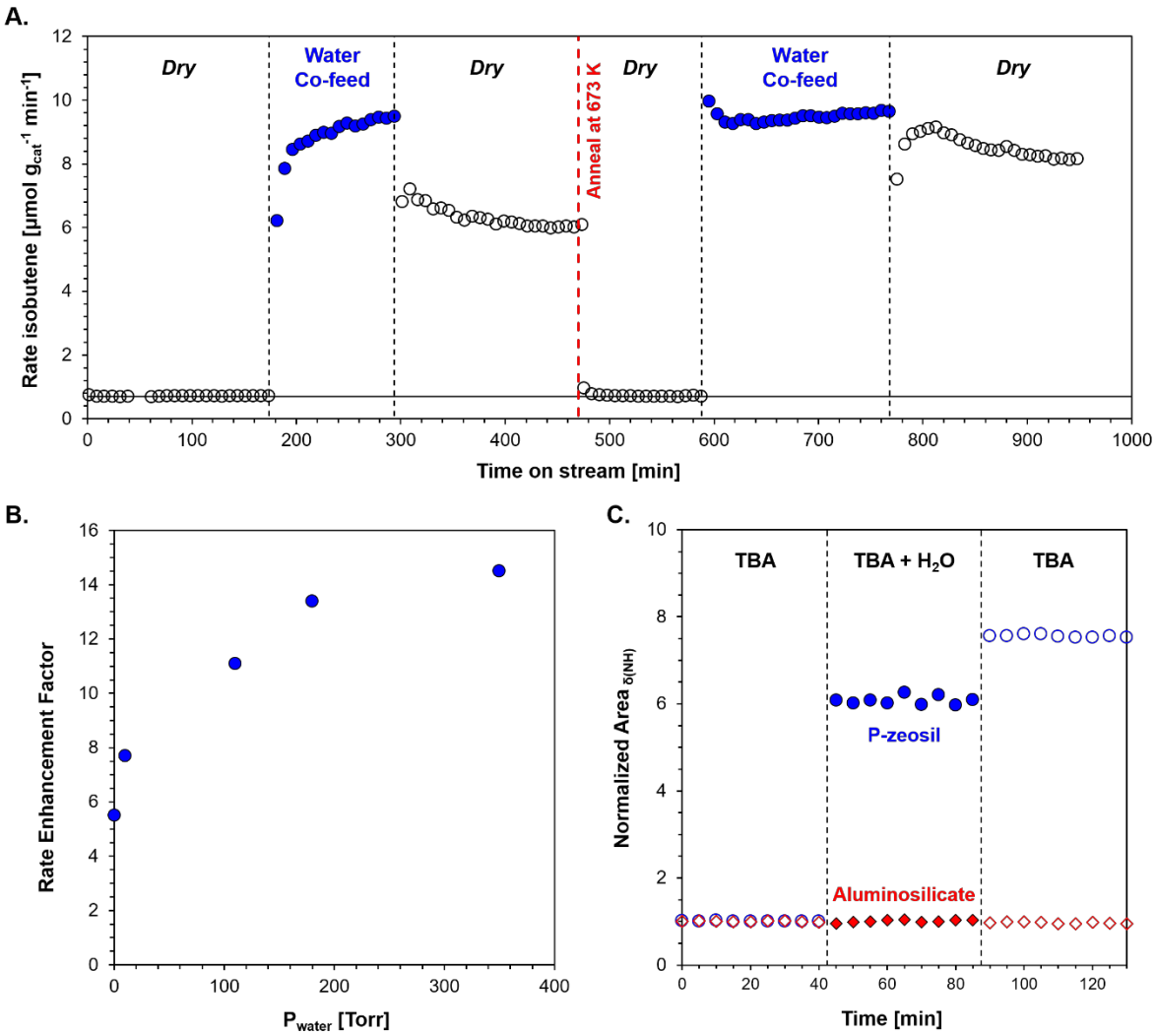

Figure 2. Effect of hydrolysis on tert-butylamine Hofmann elimination. A. Rate of Hofmann elimination in the absence and presence of 180 Torr water as a co-feed with 10 Torr tert-butylamine at 513 K. Unfilled and filled symbols represent rates measured under dry condition and water co-feed condition, respectively. The cycle was repeated by heat treating the hydrated P-BEA-3 at 673 K in He, indicated by the dashed red line **B.** Rate enhancement factor as a function of water partial pressure co-feed over TBA + water activated P-BEA-3 catalyst, with respect to rate before water was co-fed. T = 513 K, P_{TBA} = 10 Torr **C.** FT-IR integrated areas of tert-butylammonium δ(NH) deformation mode with time on stream over H-ZSM-5 (Si/Al = 11.5, ◇ / ◆) and P-BEA-3 (○ / ●) at 513 K. Integrated areas are normalized against areas before water was co-fed. Unfilled and filled symbols represent integrated areas measured under dry condition and water co-feed condition with 180 Torr of water, respectively.

3.5. P site dynamics. For the parent P-BEA-3 catalyst, in situ pyridine IR spectroscopy reveals the presence of Brønsted acid sites, indicated by the presence of protonated pyridinium (**Figure 3A**, 1542 cm^{-1}). Hydrolyzing the catalyst in water alone enhances the amount of pyridinium slightly, indicating a marginal increase in the number of Brønsted acid sites in P-BEA capable of protonating pyridine. This is in sharp contrast to the observed amount of pyridinium in P-BEA-3 after pre-treatment with tert-butylamine and water under conditions identical to those described in **Section 3.1**, where the peak area increased by more than an order of magnitude post-activation. While the parent P-BEA-3 is susceptible to hydrolysis, pre-activation with TBA appears to greatly facilitate hydrolysis on the catalyst surface, underscoring the necessity for both water and a base to effect catalyst hydrolysis and consistent with observed changes in steady-state rate measurements of 2-propanol dehydration (**Figure 1**).

To further confirm the increase in site density, as well as to capture possible effects of different activation environments, reactive gas chromatography (RGC) was performed over P-BEA-3 as an ex situ measurement of Brønsted acid site density. The principles and procedures of RGC measurements are described elsewhere.[23] When pre-treated only with a partial pressure of water equivalent to the activation procedure described in **Section 3.1** (180 Torr water), no change in the Brønsted acid site density of P-BEA-3 was observed. When pre-treated with both water and TBA simultaneously, P-BEA-3 experienced a significant increase in the number of available Brønsted acid sites (4.5x, **Figure 3B**). The lower degree of enhancement could be rationalized by the ex situ measurement conditions, which corresponds to the TBA-water-activated catalyst under dry conditions, where a 9× increase in the rate of 2-propanol dehydration was observed (**Figure 1B**).

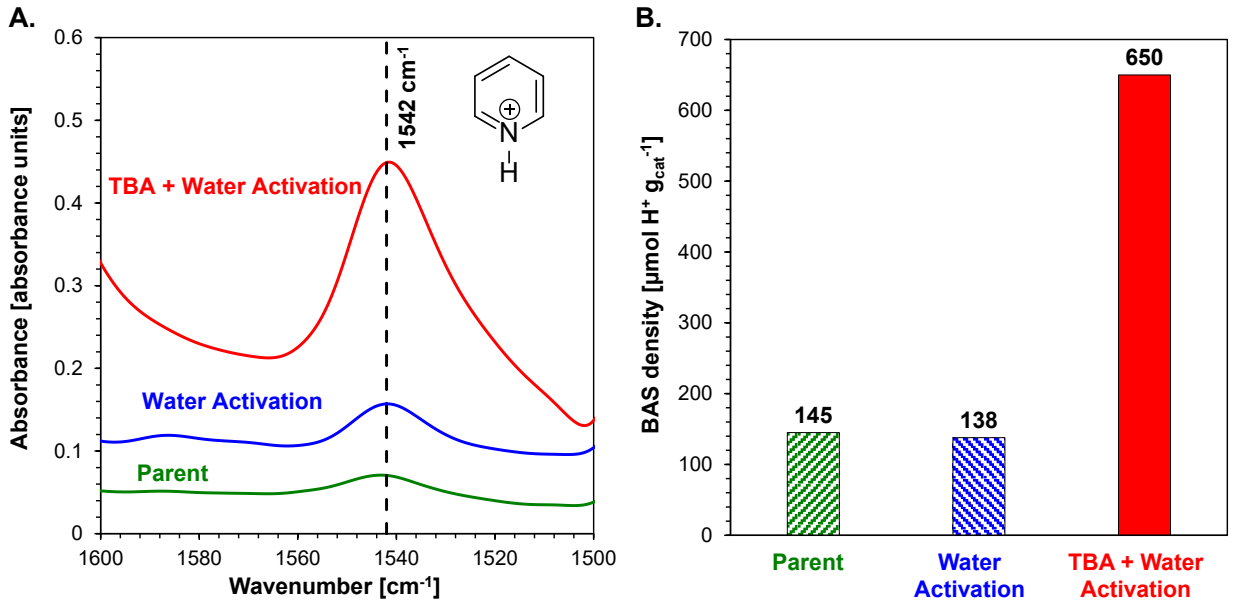

Figure 3. Acid Site Characterization of P-BEA-3. A. Pyridine IR spectra at 513 K and **B.** Ex situ measured Brønsted acid site density by reactive gas chromatography of parent (green), water-activated (blue), and TBA-water-activated (red) P-BEA-3.

3.6. P site speciation. Kinetic and spectroscopic measurements provide insights on the possible mechanism for the dynamic behavior of P-zeosils. To elucidate phosphorus site speciation before and after activation, we turned to solid-state ^{31}P nuclear magnetic resonance (NMR). Possible structures for the phosphorus sites in a P-modified self-pillared pentasil zeosil were previously elucidated by Jain et al. using solid-state ^{31}P NMR.[26] Several phosphorus species (Q^n_m) varying in the degree of P-O-P condensation (n-m) and/or Si-O-P (m) linkages were identified. The parent P-BEA-3 gives signals corresponding to an ensemble of Q^0, Q^1, Q^2, and Q^3 sites (appearing at approx. 0, -11, -24 and -43 ppm, respectively, **Figure 4**),[26] representing a distribution of surface phosphate sites with varying extents of condensation. The superscript *n* in Q^n indicates total number of P-O-X linkages with X = P or Si. We note that this nomenclature makes no distinction between P-O-Si and P-O-P linkages. The distribution of the P-sites in the parent P-BEA-3 catalyst is significantly different from P-SPP-27 reported in a previous study,[19] where most P-sites were Q^3 after the heat treatment at 723 K and 10^{-4} Torr for 12 h and P_4O_{10} was not found. In contrast, the spectrum of P-BEA-3 contains a narrow peak superposed on a broader peak in the chemical shift region corresponding to Q^3 sites, indicating two types of sites. The narrower peak corresponds to P_4O_{10},[43] while the broader peak corresponds to a distribution of framework-attached Q^3 sites with P-O-Si linkages.[26] The difference in the two materials is likely related to higher phosphorus content of P-BEA-3, or the hydrophilicity of different zeolite frameworks.

After treatment with only water (180 Torr, 513 K), P-BEA-3 continued to exhibit a prominent narrow Q^3 peak corresponding to P_4O_{10}, suggesting that water alone only hydrolyzes framework-attached Q^3 sites (P-O-Si hydrolysis, Eq. 1). The resulting Q^2 sites are seen in the increase in peak intensity at -24 ppm. However, when P-BEA-3 was exposed to a co-feed of TBA and H_2O under conditions identical to those in **Section 3.1**, where large increases in catalytic activity were observed, the Q^3 species were entirely eliminated, and predominantly Q^2 peaks were observed. Similar results were obtained when NH_3 and H_2O were co-fed, analogous to observations based on kinetic measurements, where similar enhancements in the catalytic activity of P-BEA-3 for 2-propanol dehydration were observed when pre-treated with NH_3 or TBA. Given the ex situ nature of the NMR characterization, and the dynamic nature of P-zeosils, the P-site speciation presented is most closely related to the P-BEA-3 catalyst state prior to the in situ introduction of water under reaction conditions (**Figure 1A** and **1B**, TBA + Water activation, Dry). The rate enhancement experienced as a result of base-facilitated hydrolysis therefore appears to correlate with the deconstruction of highly condensed phosphorus species on the surface of P-BEA-3; water alone is incapable of hydrolyzing on timescales relevant to the catalytic chemistry. Similarly, Qian et al. recently reported that P_4O_{10} undergoes hydrolytic ring-opening in the presence of pyridine or 4-tert-butylpyridine to form linear polyphosphates,[44] qualitatively consistent with our observation. It is possible that during the hydrolysis of P_4O_{10}, base molecules promoted the ring-opening of P_4O_{10} surface moieties, making P-O-P linkages more susceptible to nucleophilic attack by water.

P K-edge X-ray absorption near-edge structure (XANES) was also used to investigate the P-BEA samples with different Si/P ratios. P-BEA catalysts showed a decreasing absorption peak intensity with decreasing Si/P ratio, while absorption edge locations for all P-BEA samples remained constant at 2151 eV (**Supporting Information, Figure S11**), suggesting that the P oxidation state remained constant as H_3PO_4 with varying Si/P ratios. While XANES could not provide detailed P structures and their connection with the silica surface, it indicated that P-BEA with a high P loading (Si/P = 3) exhibits more condensed P structures compared to the low P loading (Si/P=27), in agreement with the observations in the ^{31}P NMR spectra.

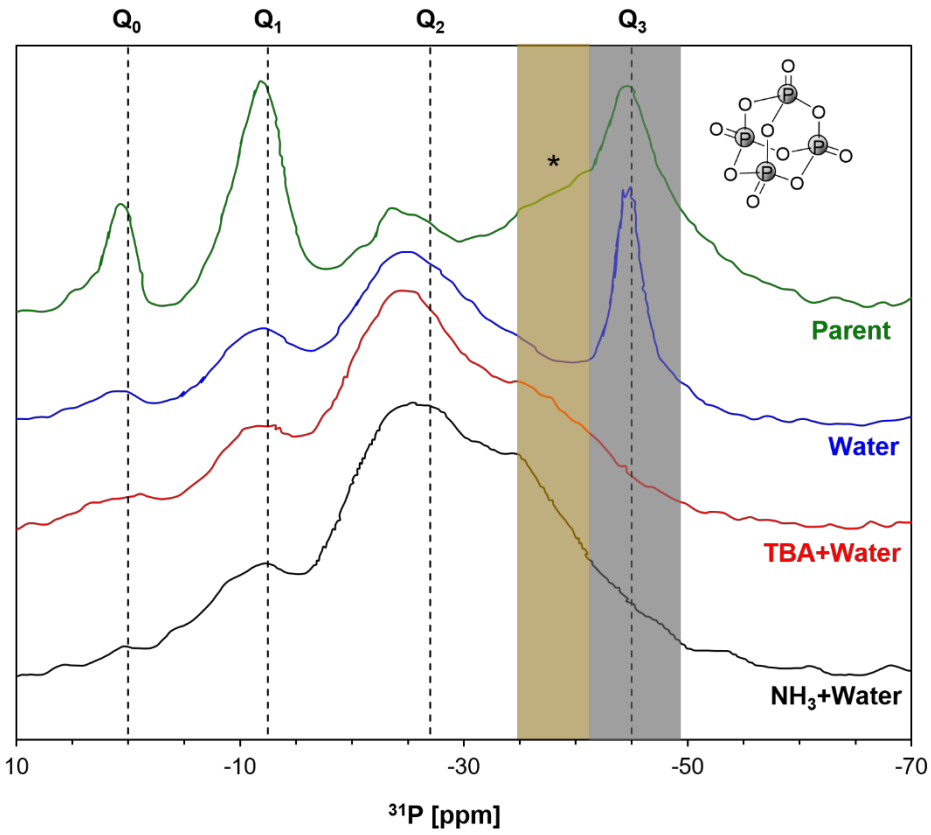

Figure 4. P site speciation of P-BEA-3. ^{31}P MAS NMR of parent (green), water-only activated (blue), TBA + water activated (red) and NH_3 + water activated P-BEA-3 catalyst (black). Catalysts were activated for 2 h using the same procedures described in previous sections. After activation, catalysts were purged in He for 2 h at 513 K to remove residual water and base molecules. The spectra were recorded at room temperature and 11.7 T magnetic field with 12.5 kHz MAS frequency. Peak shaded in orange with an asterisk (*) indicates framework-attached Q^3 sites with P-O-Si linkages, and peak shaded in gray indicates P_4O_{10}.

4. Conclusion. Our combined kinetic, synthetic, and spectroscopic investigations of P-zeosil activation through hydrolysis reveals that a base-facilitated mechanism leads to a more than two order of magnitude increase in catalytic activity. Highly condensed surface phosphorus structures limit the overall catalytic activity of P-zeosils and related catalysts but are activated with sufficiently basic molecules in the presence of water vapor. Through in situ kinetic poisoning and spectroscopic techniques, the origin of the enhancement in catalytic activity is found to be the in situ generation of Brønsted acid sites through hydrolysis of highly condensed phosphorus structures. We demonstrated that the presence of a basic molecule allows for a substantially greater extent of hydrolysis, and as a result, phosphorus-based catalysts that are more catalytically active while retaining the selective nature of their moderately acidic active sites.

Supporting Information. Details of the experimental setup, kinetic measurement of 2-propanol dehydration over Al-BEA, activation of P-BEA with only water or only TBA, rate profile during in situ poisoning for site density measurements, rate dependence of TBA Hofmann elimination

over Al-MFI and P-BEA, FT-IR spectra, XANES spectra, and elemental analysis result by XPS are available in the supporting information.

Acknowledgements. We acknowledge support from the Catalysis Center for Energy Innovation, an Energy Frontier Research Center funded by the U.S. Department of Energy, Office of Science, Office of Basic Energy Sciences, under Award number DE-SC0001004. This research used resources of the Center for Functional Nanomaterials (CFN), which is a U.S. Department of Energy Office of Science User Facility, at Brookhaven National Laboratory under Contract No. DE-SC0012704. The authors would like to acknowledge Dionisios Vlachos and Stavros Caratzoulas for helpful discussions.

References

1. A. Corma, *Chem. Rev.*, 1997, **97**, 2373-2419.
2. A. Corma, *Chem. Rev.*, 1995, **95**, 559-614.
3. M. E. Davis and R. F. Lobo, *Chem. Mater.*, 1992, **4**, 756-768.
4. M. E. Davis, *Nature*, 2002, **417**, 813-821.
5. H. J. Cho, L. Ren, V. Vattipalli, Y.-H. Yeh, N. Gould, B. Xu, R. J. Gorte, R. Lobo, P. J. Dauenhauer, M. Tsapatsis and W. Fan, *ChemCatChem*, 2017, **9**, 398-402.
6. S. Liu, T. R. Josephson, A. Athaley, Q. P. Chen, A. Norton, M. Ierapetritou, J. I. Siepmann, B. Saha and D. G. Vlachos, *Sci. Adv.*, 2019, **5**, eaav5487.
7. O. A. Abdelrahman, D. S. Park, K. P. Vinter, C. S. Spanjers, L. Ren, H. J. Cho, D. G. Vlachos, W. Fan, M. Tsapatsis and P. J. Dauenhauer, *ACS Sustainable Chem. Eng.*, 2017, **5**, 3732-3736.
8. S. Li, O. A. Abdelrahman, G. Kumar, M. Tsapatsis, D. G. Vlachos, S. Caratzoulas and P. J. Dauenhauer, *ACS Catal.*, 2019, **9**, 10279-10293.
9. P. T. M. Do, J. R. McAtee, D. A. Watson and R. F. Lobo, *ACS Catal.*, 2013, **3**, 41-46.
10. H. Kim and J. Jae, *Journal*, 2021, **11**.
11. O. A. Abdelrahman, D. S. Park, K. P. Vinter, C. S. Spanjers, L. Ren, H. J. Cho, K. Zhang, W. Fan, M. Tsapatsis and P. J. Dauenhauer, *ACS Catal.*, 2017, **7**, 1428-1431.
12. D. Mei and J. A. Lercher, *J. Phys. Chem. C*, 2019, **123**, 25255-25266.
13. K. Larmier, A. Nicolle, C. Chizallet, N. Cadran, S. Maury, A.-F. Lamic-Humblot, E. Marceau and H. Lauron-Pernot, *ACS Catal.*, 2016, **6**, 1905-1920.
14. D. T. Bregante and D. W. Flaherty, *ACS Catal.*, 2019, **9**, 10951-10962.
15. F. Cavani, G. Girotti and G. Terzoni, *Appl. Catal., A*, 1993, **97**, 177-196.
16. N. M. Prinsloo, *Fuel Processing Technology*, 2006, **87**, 437-442.
17. H. Chen and O. A. Abdelrahman, *ACS Catal.*, 2021, **11**, 6416-6430.
18. J. S. Bates, B. C. Bukowski, J. Greeley and R. Gounder, *Chem. Sci.*, 2020, **11**, 7102-7122.
19. Y. Zhi, H. Shi, L. Mu, Y. Liu, D. Mei, D. M. Camaioni and J. A. Lercher, *J. Am. Chem. Soc.*, 2015, **137**, 15781-15794.
20. J. Gulbinski, L. Ren, V. Vattipalli, H. Chen, J. Delaney, P. Bai, P. Dauenhauer, M. Tsapatsis, O. A. Abdelrahman and W. Fan, *Ind. Eng. Chem. Res.*, 2020, **59**, 22049-22056.
21. P. Northrup, *J. Synchrotron Rad.*, 2019, **26**, 2064-2074.
22. O. Bunău and Y. Joly, *J. Phys. Condens. Matter*, 2009, **21**, 345501.

23. O. A. Abdelrahman, K. P. Vinter, L. Ren, D. Xu, R. J. Gorte, M. Tsapatsis and P. J. Dauenhauer, *Catal. Sci. Technol.*, 2017, **7**, 3831-3841.
24. G. Kumar, L. Ren, Y. Pang, X. Li, H. Chen, J. Gulbinski, P. J. Dauenhauer, M. Tsapatsis and O. A. Abdelrahman, *ACS Catal.*, 2021, **11**, 9933-9948.
25. J. Zhang, Y. Yan, Q. Chu and J. Feng, *Fuel Process. Technol.*, 2015, **135**, 2-5.
26. S. K. Jain, T. Tabassum, L. Li, L. Ren, W. Fan, M. Tsapatsis, S. Caratzoulas, S. Han and S. L. Scott, *J. Am. Chem. Soc.*, 2021, **143**, 1968-1983.
27. W. Dall'Acqua and P. Carter, *Protein Sci.*, 2000, **9**, 1-9.
28. S. Jonas and F. Hollfelder, *Pure Appl. Chem.*, 2009, **81**, 731-742.
29. F. Duarte, J. Åqvist, N. H. Williams and S. C. L. Kamerlin, *J. Am. Chem. Soc.*, 2015, **137**, 1081-1093.
30. A. J. Kirby, M. Medeiros, J. R. Mora, P. S. M. Oliveira, A. Amer, N. H. Williams and F. Nome, *J. Org. Chem.*, 2013, **78**, 1343-1353.
31. S. B. B. B. Bahia, C. A. Amaya Vargas, Â. M. L. Denadai, M. H. Araujo, A. H. Moraes and T. A. S. Brandão, *J. Phys. Chem. C*, 2020, **124**, 17111-17120.
32. R. T. Carr, M. Neurock and E. Iglesia, *J. Catal.*, 2011, **278**, 78-93.
33. C. P. Nash, A. Ramanathan, D. A. Ruddy, M. Behl, E. Gjersing, M. Griffin, H. Zhu, B. Subramaniam, J. A. Schaidle and J. E. Hensley, *Appl. Catal., A*, 2016, **510**, 110-124.
34. L. V. Malysheva, E. A. Paukshtis and N. S. Kotsarenko, *J. Catal.*, 1987, **104**, 31-36.
35. W. E. Farneth and R. J. Gorte, *Chem. Rev.*, 1995, **95**, 615-635.
36. D. R. Lide, *CRC Handbook of Chemistry and Physics*, CRC Press, Internet Version 2005 edn., 2005.
37. D. J. Parrillo, A. T. Adamo, G. T. Kokotailo and R. J. Gorte, *Appl. Catal.*, 1990, **67**, 107-118.
38. C. R. Ho, L. A. Bettinson, J. Choi, M. Head-Gordon and A. T. Bell, *ACS Catal.*, 2019, **9**, 7012-7022.
39. G. Busca, G. Ramis, V. Lorenzelli, P. F. Rossi, A. La Ginestra and P. Patrono, *Langmuir*, 1989, **5**, 911-916.
40. M. J. D. Low and P. Ramamurthy, *J. Phys. Chem.*, 1968, **72**, 3161-3167.
41. R. M. Ravenelle, F. Schüβler, A. D'Amico, N. Danilina, J. A. van Bokhoven, J. A. Lercher, C. W. Jones and C. Sievers, *J. Phys. Chem. C*, 2010, **114**, 19582-19595.
42. S. Prodinger and M. A. Derewinski, *Pet. Chem.*, 2020, **60**, 420-436.
43. G. Jeschke, W. Hoffbauer and M. Jansen, *Chem. Eur. J.*, 1998, **4**, 1755-1761.
44. K. Qian, S. M. Shepard, T. Xin, G. Park and C. C. Cummins, *J. Am. Chem. Soc.*, 2023, **145**, 6045-6050.